Title

Coherent ambient infrasound recorded by the International Monitoring System

Journal

Geophys. Res. Lett., 40

Authors

Matoza, Robin S

Landès, Matthieu

Le Pichon, Alexis

et al.

Publication Date

2013-01-28

Peer reviewed

Coherent ambient infrasound recorded by the International Monitoring System

Robin S. Matoza,[1,2] Matthieu Landès,[1] Alexis Le Pichon,[1] Lars Ceranna,[3] and David Brown[4]

Received 22 October 2012; revised 4 December 2012; accepted 4 December 2012.

[1] The ability of the International Monitoring System (IMS) infrasound network to detect atmospheric nuclear explosions and other signals of interest is strongly dependent on station-specific ambient noise. This ambient noise includes both incoherent wind noise and real coherent infrasonic waves. Previous ambient infrasound noise models have not distinguished between incoherent and coherent components. We present a first attempt at statistically and systematically characterizing coherent infrasound recorded by the IMS. We perform broadband (0.01–5 Hz) array processing with the IMS continuous waveform archive (39 stations from 1 April 2005 to 31 December 2010) using an implementation of the Progressive Multi-Channel Correlation algorithm in log-frequency space. From these results, we estimate multi-year 5th, 50th, and 95th percentiles of the RMS pressure of coherent signals in 15 frequency bands for each station. We compare the resulting coherent infrasound models with raw power spectral density noise models, which inherently include both incoherent and coherent components. Our results indicate that IMS arrays consistently record coherent ambient infrasound across the broad frequency range from 0.01 to 5 Hz when wind noise levels permit. The multi-year averaging emphasizes continuous signals such as oceanic microbaroms, as well as persistent transient signals such as repetitive volcanic, surf, thunder, or anthropogenic activity. Systematic characterization of coherent infrasound detection is important for quantifying a station's recording environment, signal-to-noise ratio as a function of frequency and direction, and overall performance, which all influence the detection probability of specific signals of interest.
Citation: Matoza, R. S., Landès, M., Le Pichon, A., Ceranna, L., and Brown, D. (2013), Coherent ambient infrasound recorded by the International Monitoring System, *Geophys. Res. Lett. 40,* doi: 10.1029/2012GL054329.

1. Introduction

[2] The International Monitoring System (IMS) global infrasonic network is designed to detect atmospheric nuclear explosions anywhere on the planet [*Christie and Campus*, 2010]. The network also has potential application in monitoring natural hazards such as large volcanic explosions [*Matoza et al*., 2011] and severe weather [*Hetzer et al*., 2008]. The capability of the IMS infrasonic network to detect signals of interest exhibits significant spatiotemporal variation, which is in part controlled by station-specific ambient infrasonic noise [*Le Pichon et al*., 2009; *Green and Bowers*, 2010].

[3] Each station of the IMS infrasonic network is a microbarometer or microphone array, with at least four sensor elements spatially separated with apertures of up to a few kilometers. The arrays are designed such that wind noise will be incoherent (not spatially correlated) between elements, while real acoustic waves will be coherent (spatially correlated).

[4] Wind is the dominant noise source in the frequency band 0.01–5 Hz [*Walker and Hedlin*, 2010]. At a given infrasound station, wind variations can account for 4 orders of magnitude difference in the background noise power spectral density (PSD) at a particular frequency [*Hedlin et al*., 2002; Bowman *et al*., 2005; *Brown et al*., 2011]. Wind noise PSD probability varies with time of day, season, and geographic location [*Bowman et al*., 2005]. Previous IMS infrasound noise studies [e.g., *Bowman et al*., 2005] have considered raw ambient PSD probability without distinguishing between incoherent wind noise and ambient coherent infrasonic signals generated by repetitive natural or anthropogenic processes. However, it is well known that repetitive coherent infrasonic signals (sometimes called "clutter") present practical constraints on identifying target infrasonic signals of interest [e.g., *Evers and Haak*, 2001; *Hetzer and Waxler*, 2009].

[5] Here we present summary statistics of coherent infrasound recorded by the IMS network during 2005–2010, identified by systematic broadband (0.01 to 5 Hz) array processing. Our work represents a first attempt at statistically and systematically characterizing coherent ambient infrasound recorded by the IMS.

2. Data and Methods

[6] We consider data from 39 IMS infrasound stations (Figures 1a and 1b) from 1 April 2005 to 31 December 2010. The 39 stations represent the 42 IMS stations certified as of 1 December 2010 minus 3 stations for which problems were encountered with metadata or data availability. Since the IMS network is currently under construction, data availability varies throughout the time period considered (Figure 1b). Each station consists of an array of at least four sensors with a flat response from 0.01 to 8 Hz (sampled at 20 Hz) and a sensitivity of about 0.1 mPa/count. Array aperture, geometry, and number of elements (Figure 1a) varies between stations of the IMS network [*Christie and Campus*, 2010]; this is the principal limitation to systematic data analysis. However, in aiming to make our results as comparable as possible between stations, we perform data processing with the same parameters for all stations.

[7] We perform array processing using the Progressive Multi-Channel Correlation algorithm (PMCC) [*Cansi*, 1995]. PMCC estimates wavefront parameters (e.g., back azimuth,

[1]CEA/DAM/DIF, Arpajon, France.
[2]Institute of Geophysics and Planetary Physics, Scripps Institution of Oceanography, University of California, San Diego, La Jolla, California, USA.
[3]BGR, Hannover, Germany.
[4]CTBTO, Vienna, Austria.

Corresponding author: R. S. Matoza, Institute of Geophysics and Planetary Physics, Scripps Institution of Oceanography, University of California, San Diego, La Jolla, CA 92093-0225, USA. (rmatoza@ucsd.edu)

/0094-8276/13/10.1029/2012GL054329,

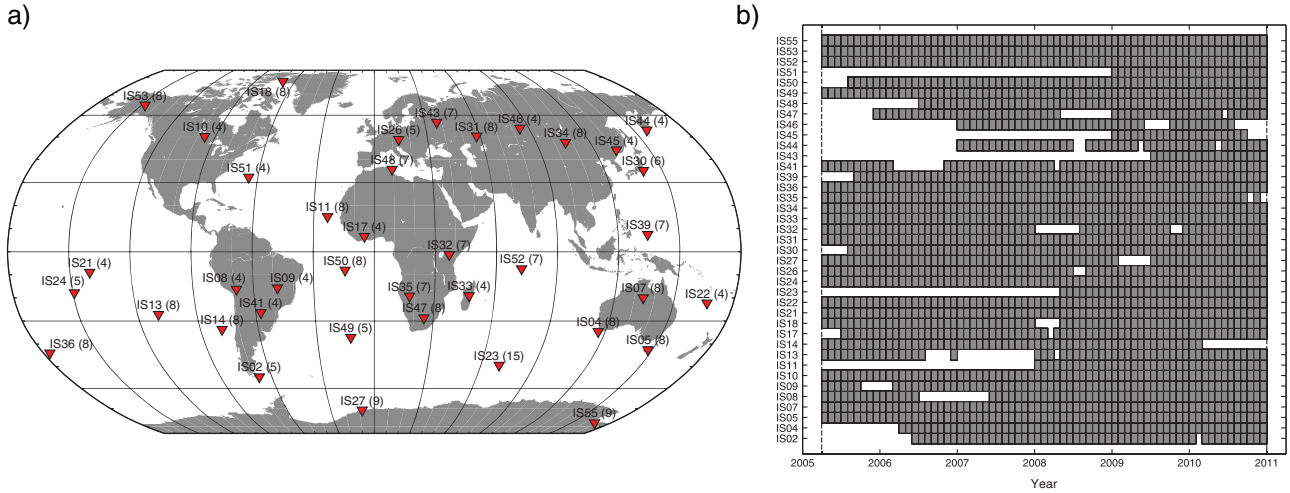

Figure 1. (a) Map of 39 IMS infrasound stations (red inverted triangles) considered in this study. Number of array elements at each station is in parentheses. (b) Data availability at the 39 stations between 1 April 2005 and 31 December 2010 (vertical dashed lines). Gray boxes correspond to months during which at least one PMCC detection (pixel) was registered at the station indicated on the vertical axis. Data availability before 1 April 2005 and after 31 December 2010 is not shown.

apparent velocity, root-mean-square amplitude) of coherent plane waves in a given time window using correlation time delays between successive array element triplets or sub-networks [*Cansi*, 1995]. PMCC performs a grid search for coherent signals in advancing time windows over a set of frequency bands defined with band-pass filters (Table 1). PMCC records the wavefront properties of the dominant coherent arrival in a given time-window and frequency-band pair as a *pixel*. PMCC then groups pixels with similar wavefront properties into *families* [*Cansi and Klinger*, 1997]. We implement PMCC here in 15 log-spaced frequency bands defined with Chebyshev filters of order 2 between 0.01 and 5 Hz (Table 1). We vary the time-window length in proportion to 1/frequency from 200 s to 30 s; the window is advanced in time steps 10% of the window length (Table 1). The use of log-spaced frequency bands permits computationally efficient broadband processing and helps with signal discrimination [*Brachet et al.*, 2010; *Le Pichon et al.*, 2010]. Because we are interested in signals with frequencies as low as 0.01 Hz, we choose sub-network geometries to exploit the maximum array element separations at each array. We only keep signals that have apparent velocities between 0.3 and 0.5 km/s.

Table 1. PMCC array processing time-window and frequency-band configurations

Band #	$f_{\min}$ [Hz]	f_{center} [Hz]	$f_{\max}$ [Hz]	Window Length [s]	Time Step [s]
1	0.0100	0.0126	0.0151	200.0000	20.0000
2	0.0151	0.0190	0.0229	142.1606	14.2161
3	0.0229	0.0288	0.0347	103.9404	10.3940
4	0.0347	0.0436	0.0524	78.6846	7.8685
5	0.0524	0.0659	0.0794	61.9956	6.1996
6	0.0794	0.0997	0.1201	50.9676	5.0968
7	0.1201	0.1509	0.1818	43.6803	4.3680
8	0.1818	0.2284	0.2751	38.8648	3.8865
9	0.2751	0.3457	0.4163	35.6828	3.5683
10	0.4163	0.5231	0.6300	33.5801	3.3580
11	0.6300	0.7916	0.9533	32.1907	3.2191
12	0.9533	1.1980	1.4427	31.2725	3.1273
13	1.4427	1.8130	2.1833	30.6658	3.0666
14	2.1833	2.7436	3.3040	30.2649	3.0265
15	3.3040	4.1520	5.0000	30.0000	3.0000

[8] To summarize the large number of resulting PMCC pixels, we estimate 5th, 50th, and 95th percentiles of the root-mean-square pressure $p_{\text{RMS}}^{\text{PMCC}}$ [Pa] in each frequency band. This summarizes the multi-year (2005–2010) PMCC results at each station by 3 percentile curves, each with 15 values of $p_{\text{RMS}}^{\text{PMCC}}$ centered on the band center frequencies (Figure 2). Although we estimate the percentiles directly from the PMCC pixels, we only use PMCC pixels that have been automatically grouped into families [*Cansi and Klinger*, 1997], greatly reducing the potential contribution from non-physical spuriously correlated signals.

[9] We compare the PMCC results with raw power spectral density (PSD) [Pa^2/Hz] curves for each station obtained independently by *Brown et al.* [2011]. *Brown et al.* [2011] estimated the PSD for every hour of data in year 2010 on each element of every available IMS station using Welch's periodogram method. The sub-window length used for the PSDs is 300 s; assuming 10 cycles for a reliable PSD, this should yield accurate results down to 30 s period, that is, ~0.03 Hz. Data availability for the PSD estimates in 2010 is similar to that represented in Figure 1b. To facilitate comparison with the PMCC results, we integrate the PSD curves, $S(f)$, across each frequency band (Table 1) used in the PMCC processing:

$$\left(p_{\text{RMS}}^{\text{PSD}}\right)^2 = \int_{f_{\min}}^{f_{\max}} S(f)\,\mathrm{d}f, \tag{1}$$

where f is the frequency; $f_{\min}$ and $f_{\max}$ are the lower and upper frequencies, respectively, defining each frequency band (Table 1); and $p_{\text{RMS}}^{\text{PSD}}$ is the root-mean-square pressure [Pa] in the frequency band between $f_{\min}$ and $f_{\max}$. We estimate the 5th, 50th, and 95th percentiles of the resulting $p_{\text{RMS}}^{\text{PSD}}$ curves for year 2010 (estimating first over every 24 h and then over the 365 days in the year), resulting in 3 final $p_{\text{RMS}}^{\text{PSD}}$ curves of 15 values for each station (Figure 2).

3. Results

[10] Figure 2 shows the resulting coherent infrasound $\left(p_{\text{RMS}}^{\text{PMCC}}\right)$ and raw noise $\left(p_{\text{RMS}}^{\text{PSD}}\right)$ curves for 3 example stations

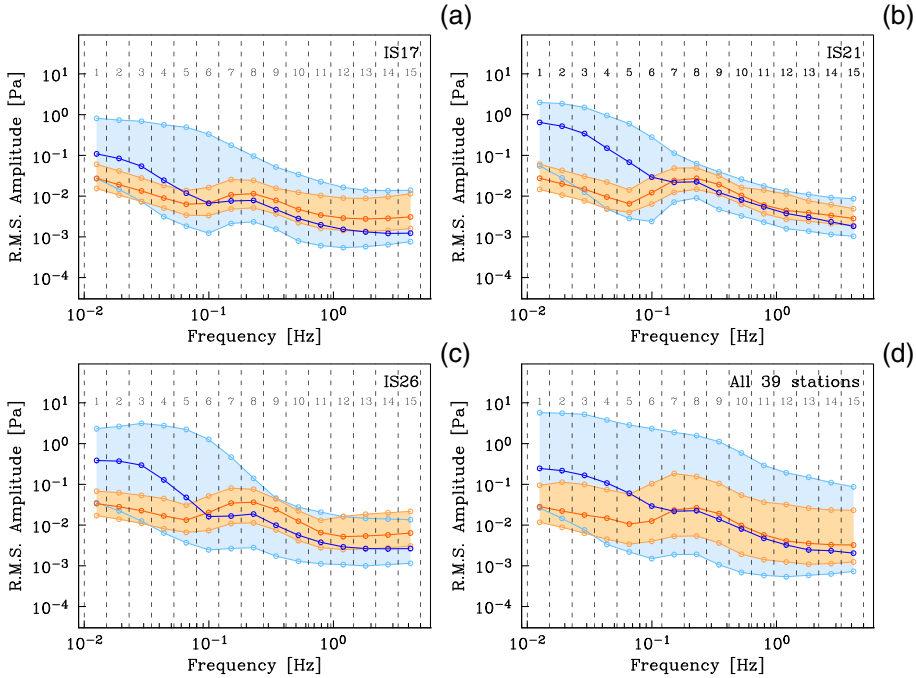

Figure 2. Coherent infrasound (orange) compared with raw noise (blue) RMS pressure for 3 example stations (a) IS17, (b) IS21, and (c) IS26 (station name indicated in upper right of each plot) and for (d) a summary of all 39 stations. In each case, we show 3 curves of $p_{\mathrm{RMS}}^{\mathrm{PMCC}}$ (orange) and $p_{\mathrm{RMS}}^{\mathrm{PSD}}$ (blue). In Figures 2a–2c, the 3 curves are the 5th, 50th, and 95th percentiles. In Figure 2d, the 3 curves are the 5th, 50th, and 95th percentiles of all 39 stations' individual 5th, 50th, and 95th percentile curves. Each curve consists of 15 points plotted at the band center frequency (Table 1). Vertical dashed lines indicate the frequency bands (f_{min} and f_{max}). The $p_{\mathrm{RMS}}^{\mathrm{PMCC}}$ (orange) curves are estimated for data from 1 April 2005 to 31 December 2010. The $p_{\mathrm{RMS}}^{\mathrm{PSD}}$ (blue) curves are estimated for data from 1 January 2010 to 31 December 2010. Similar individual plots for all 39 stations are included in the Auxiliary Material (Figure S1).

and a summary of all 39 stations. Individual plots for all 39 stations are provided in the Auxiliary Material (Figure S1). Comparison of $p_{\mathrm{RMS}}^{\mathrm{PMCC}}$ with $p_{\mathrm{RMS}}^{\mathrm{PSD}}$ permits identification of which regions of the raw noise PSD curves are controlled by coherent ambient infrasound. A striking result of our analysis is that coherent infrasound is consistently identified across the broad frequency range from 0.01 to 5 Hz at every station of the IMS network (Figure 2; Figure S1). At each station, the coherent infrasound curves can be approximately divided into three distinct frequency ranges: (i) 0.01–0.08 Hz, (ii) 0.08–0.5 Hz, and (iii) 0.5–5 Hz. Microbaroms [*Waxler and Gilbert*, 2006] dominate the band 0.08–0.5 Hz, with amplitude peaked at ~0.2 Hz in each case. Signals in the band 0.5–5 Hz likely result from a variety of sources occurring at local and regional distances from each array. Our averaging process emphasizes continuous or repetitive signals. Examples of known repetitive signals recorded in the 0.5–5 Hz band at IMS stations include surf [*Garces et al.*, 2003; *Le Pichon et al.*, 2004], thunder [*Farges and Blanc*, 2010], volcanoes [*Le Pichon et al.*, 2005], and anthropogenic activity (e.g., mining, industrial activity, aircraft, or urban noise) [*Le Pichon et al.*, 2008]. The consistent identification of coherent signals in the 0.01–0.08 Hz band (orange curves; Figure 2; Figure S1) is an interesting result because this band is largely dominated by wind noise (blue curves; Figure 2; Figure S1). Examples of potential repetitive sources in this band include Mountain Associated Waves (MAW) and, at high latitudes, geomagnetic and auroral activity [*Bedard and Georges*, 2000; *Wilson et al.*, 2010].

[11] The signal-to-noise ratio implied between $p_{\mathrm{RMS}}^{\mathrm{PMCC}}$ and $p_{\mathrm{RMS}}^{\mathrm{PSD}}$ at frequencies of 0.01–0.08 Hz is very low (~0.01–0.1; Figure 2; Figure S1); it is lower than we would expect from the PMCC algorithm. Numerical experiments indicate that PMCC detects signals with signal-to-noise ratios as low as between 0.15 and 0.5 [*Cansi et al.*, 2005]. The $p_{\mathrm{RMS}}^{\mathrm{PMCC}}$ curves fall below the 5th percentile $p_{\mathrm{RMS}}^{\mathrm{PSD}}$ at frequencies of ~0.01–0.05 Hz. However, the number of coherent detections is strongly frequency dependent (Figure 3; Figure S1). Figure 3 shows summaries of the number of pixels per month (N) at the same example stations (Figures 3a–3c) and a summary of all 39 stations (Figure 3d). The absolute value of N depends on our choice of detection parameters, particularly on the time-window length and number of frequency bands (Table 1). However, because we systematically use the same detection parameters for all stations, N is a useful metric to compare the relative number of coherent detections at different stations.

[12] At IS26 (Figure 3c), there are ~2 orders of magnitude more detections in the microbarom band (0.08–0.5 Hz) than in the low-frequency band (0.01–0.08 Hz). The median value of N for all stations in band #2 (Table 1; Figure 3d) corresponds to only about 10 pixels per day, which is a very low value. This indicates that the $p_{\mathrm{RMS}}^{\mathrm{PMCC}}$ statistics are highly undersampled compared to the $p_{\mathrm{RMS}}^{\mathrm{PSD}}$ statistics at low frequencies in Figure 2. The simplest interpretation of the behavior at 0.01–0.08 Hz in Figures 2 and 3 is that PMCC detections are only registered when wind noise levels are low enough, including times when the noise is below the 5th percentile.

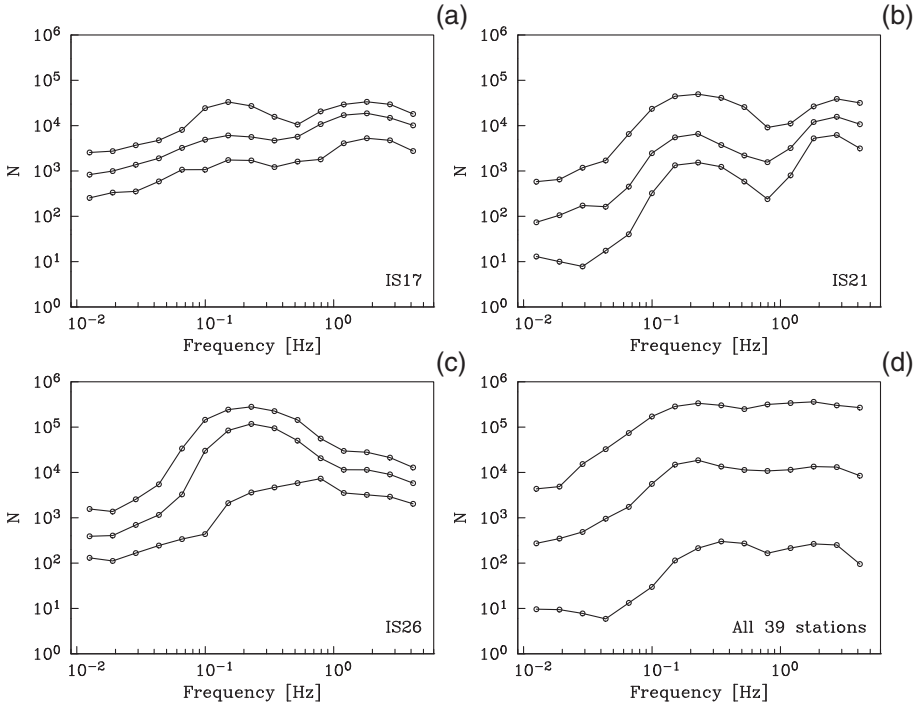

Figure 3. Number of coherent PMCC pixels detected per month (N) at 3 example stations (a) IS17, (b) IS21, and (c) IS26 (station name indicated in lower right of each plot) and for (d) a summary of all 39 stations. In Figures 3a–3c, the 3 curves are the 5th, 50th, and 95th percentile curves of N in the 15 bands plotted at the band center frequency (Table 1). In Figure 3d, the 3 curves are the 5th, 50th, and 95th percentiles of all 39 stations' individual 5th, 50th, and 95th percentile curves. Similar individual plots for all 39 stations are included in the Auxiliary Material (Figure S2).

4. Discussion and Conclusions

[13] Our study represents a first attempt at statistically and systematically characterizing coherent ambient infrasound as recorded by the IMS network across a broad bandwidth. Coherent ambient infrasound detection models such as these could be used to make more accurate and realistic infrasonic network detection capability models [*Le Pichon et al*., 2009; *Green and Bowers*, 2010]. For operational purposes, our results (e.g., Figures 2 and 3) also permit relative comparisons of stations' ambient coherent infrasound amplitudes and overall station performance characteristics (e.g., number of detections per band). More fundamentally, our results indicate the global ubiquity of atmospheric infrasound waves in the band from 0.01 to 5 Hz.

[14] We note that *Gossard* [1960] studied the composition of atmospheric pressure spectra using long-duration barometric time series and proposed power-law fits to the frequency dependence. Our results are not consistent with Gossard's due to the presence of microbaroms in our frequency band; however, comparing our results with power laws may be an interesting avenue for further research.

[15] We identify some limitations to our current approach. The PMCC RMS pixel amplitude is calculated as the RMS amplitude of the waveform (signal + uncorrelated noise) in the time window and frequency band pass, averaged across all contributing channels. Thus, in cases of low signal-to-noise ratio, the reported amplitudes may be influenced by uncorrelated noise. Steps could be taken to account for this in future work.

[16] It is difficult to establish with confidence that the signals in the 0.01–0.08 Hz band (Figure 2) are real signals because of the relatively low numbers of detections (Figure 3). Quantification of the false alarm rate of the PMCC detector [*Charbit et al*., 2012] is required before we can fully establish the detections in the 0.01–0.08 Hz band as real infrasonic signals. However, these signals often occur in temporal patterns [e.g., they occur in austral winter with a consistent back azimuth at IS22; *Le Pichon et al*., 2010]. The signals have also been detected and studied independently using other array processing techniques [e.g., *Wilson et al*., 2010], suggesting that they are real signals.

[17] Although $p^{\mathrm{PSD}}_{\mathrm{RMS}}$ and $p^{\mathrm{PMCC}}_{\mathrm{RMS}}$ have comparable units, they will not necessarily be equal for an observed signal. Ambient infrasound includes both continuous signals [e.g., microbaroms; *Donn and Rind*, 1971] and repetitive pulse-like signals [e.g., surf; *Le Pichon et al*., 2004]. For continuous, stationary signals, $p^{\mathrm{PSD}}_{\mathrm{RMS}}$ and $p^{\mathrm{PMCC}}_{\mathrm{RMS}}$ will have similar values, as seen for the micro-barom peak in Figure 2. However, for pulse-like signals whose duration is shorter than the data processing window lengths (Table 1), the assumption of stationarity is violated and both $p^{\mathrm{PMCC}}_{\mathrm{RMS}}$ and $p^{\mathrm{PSD}}_{\mathrm{RMS.}}$ will underestimate the signal amplitude. Because 300 s sub-windows were used in the PSD estimation, multiple pulse-like signals may be contained in a PSD estimate and their energy would be averaged across the time window. Similarly, PMCC window lengths may sample multiple impulse signals or a fraction of a full signal. $p^{\mathrm{PMCC}}_{\mathrm{RMS}}$ is a good estimate of the signal amplitude only when the window length approximates the signal duration. Quantitative comparison between $p^{\mathrm{PSD}}_{\mathrm{RMS}}$ and $p^{\mathrm{PMCC}}_{\mathrm{RMS}}$ for repetitious pulse-like signals such as surf is therefore not straightforward and beyond the scope of the present work.

[18] However, these limitations are not typically addressed in raw infrasound PSD noise models [*Bowman et al*., 2005; *Brown et al*., 2011]. In addition, PMCC is the signal detector

in use by the International Data Center (IDC) of the Comprehensive nuclear Test-Ban Treaty Organization (CTBO), and signals of interest must be identified within these ambient repetitive coherent detections [*Brachet et al*., 2010]. Our results therefore represent a summary of ambient coherent infrasound similar to how it is detected in practice.

[19] Our results are also somewhat dependent on the number and width of frequency bands (Table 1). A practical improvement could be made by defining standard frequency bands for use in the infrasound research community. For example, ANSI standard one-third octave bands [*ANSI*, 2004] could be extended down into the infrasound frequency range, and standard filter performance requirements could be defined for infrasound data.

[20] For simplicity, we have chosen to summarize the multiyear (2005–2010) array processing results by three curves at each station; however, this does not exploit the full utility of array processing. The PMCC results include information on the azimuth and apparent velocity of the coherent signals, which typically exhibit systematic seasonal variations [*Le Pichon et al*., 2009]. These systematic seasonal variations result from changes in both the source distribution [e.g., *Landes et al*., 2012] and atmospheric waveguides [e.g., *Le Pichon et al*., 2005; *Evers and Siegmund*, 2009; *Drob et al*., 2010] and could likely be characterized statistically. Diurnal variations, for example, in anthropogenic activity, or resulting from boundary layer effects [e.g., *Fee and Garces*, 2007] or solar tides [e.g., *Assink et al*., 2012], could also potentially be characterized. Therefore, the probable look directions and frequencies that are continuously obscured by background detections, along with their power levels, could be quantified for each IMS array as a function of time.

[21] **Acknowledgments.** We thank the IDC of the CTBTO for data access and Milton Garces for suggesting the use of ANSI standard frequency bands. The PMCC software is developed and maintained by the CEA. We thank Läslo Evers and Stephen Arrowsmith for their reviews, which helped us to improve the manuscript. Our noise curves are available for download at http://igppweb.ucsd.edu/~rmatoza.

References

ANSI (2004), Octave-band and fractional-octave-band analog and digital filters, American National Standard, ANSI/ASA S1.11-2004 (R2009).

Assink, J. D., R. Waxler, and D. Drob (2012), On the sensitivity of infrasonic traveltimes in the equatorial region to the atmospheric tides, *J. Geophys. Res.*, *117*, D01110, doi:doi:10.1029/2011JD016107.

Bedard, A. J., and T. M. Georges (2000), Atmospheric infrasound, *Phys. Today*, *53*(3), 32–37.

Bowman, J. R., G. E. Baker, and M. Bahavar (2005), Ambient infrasound noise, *Geophys. Res. Lett.*, *32*, L09803, doi:doi:10.1029/2005GL022486.

Brachet, N., D. Brown, R. Le Bras, Y. Cansi, P. Mialle, and J. Coyne (2010), Monitoring the Earth's atmosphere with the global IMS infrasound network, in *Infrasound Monitoring for Atmospheric Studies*, edited by A. L. Pichon, E. Blanc, and A. Hauchecorne, chap. 3, pp. 77–118, Springer, Netherlands.

Brown, D., L. Ceranna, M. Prior, P. Mialle, and R. Le Bras (2011), The IDC seismic, hydroacoustic and infrasound global low and high noise models, Infrasound Technology Workshop, Jordan.

Cansi, Y. (1995), An automatic seismic event processing for detection and location: The P.M.C.C. method, *Geophys. Res. Lett.*, *22*(9), 1021–1024.

Cansi, Y., and Y. Klinger (1997), An automated data processing method for mini-arrays, *CSEM/EMSC Newsletter*, *11*, 2–4.

Cansi, Y., J. Vergoz, and E. Schissele-Rebel (2005), A quantitative evaluation of P.M.C.C.'s detection capability, paper presented at the Infrasound Technology Workshop, Tahiti, French Polynesia.

Charbit, M., P. Gaillard, and A. Le Pichon (2012), Evaluating the performance of infrasound detectors, paper presented at the EGU General Assembly, Vienna, Austria.

Christie, D., and P. Campus (2010), The IMS infrasound network: Design and establishment of infrasound stations, in *Infrasound Monitoring for Atmospheric Studies*, edited by A. L. Pichon, E. Blanc, and A. Hauchecorne, chap. 2, pp. 29–75, Springer, Netherlands.

Donn, W. L., and D. Rind (1971), Natural infrasound as an atmospheric probe, *Geophys. J. R. Astr. Soc.*, *26*, 111–133.

Drob, D. P., M. Garces, M. Hedlin, and N. Brachet (2010), The temporal morphology of infrasound propagation, *Pure Appl. Geophys.*, *167*(4–5), 437–453, doi:10.1007/s00024-010-0080-6.

Evers, L. G., and H. W. Haak (2001), Listening to sounds from an exploding meteor and oceanic waves, *Geophys. Res. Lett.*, *28*(1), 41–44, doi:10.1029/2000GL011859.

Evers, L. G., and P. Siegmund (2009), Infrasonic signature of the 2009 major sudden stratospheric warming, *Geophys. Res. Lett.*, *36*, L23808, doi:10.1029/2009GL041323.

Farges, T., and E. Blanc (2010), Characteristics of infrasound from lightning and sprites near thunderstorm areas, *J. Geophys. Res.*, *115*, A00E31, doi:10.1029/2009JA014700.

Fee, D., and M. Garces (2007), Infrasonic tremor in the diffraction zone, *Geophys. Res. Lett.*, *34*, L16826, doi:10.1029/2007GL030616.

Garces, M., C. Hetzer, M. Merrifield, M. Willis, and J. Aucan (2003), Observations of surf infrasound in Hawai'i, *Geophys. Res. Lett.*, *30*(24), 2264, doi:10.1029/2003GL018614.

Gossard, E. E. (1960), Spectra of atmospheric scalars, *J. Geophys. Res.*, *65* (10), 3,339–3,351.

Green, D. N., and D. Bowers (2010), Estimating the detection capability of the International Monitoring System infrasound network, *J. Geophys. Res.*, *115*, D18116, doi:10.1029/2010JD014017.

Hedlin, M. A. H., J. Berger, and F. Vernon (2002), Surveying infrasonic noise on oceanic islands, *Pure Appl. Geophys.*, *159*, 1127–1152.

Hetzer, C., and R. Waxler (2009), Development and application of first- and second-pass clutter-reduction techniques for nuclear blast detection at infrasound stations, AGU Fall Meeting, S31B-1720.

Hetzer, C. H., R. Waxler, K. E. Gilbert, C. L. Talmadge, and H. E. Bass (2008), Infrasound from hurricanes: Dependence on the ambient ocean surface wave field, *Geophys. Res. Lett.*, *35*, L14609, doi:10.1029/2008GL034614.

Landès, M., L. Ceranna, A. Le Pichon, and R. S. Matoza (2012), Localization of microbarom sources using the IMS infrasound network, *J. Geophys. Res.*, *117*, D06102, doi:10.1029/2011JD016684.

Le Pichon, A., V. Maurer, D. Raymond, and O. Hyvernaud (2004), Infrasound from ocean waves observed in Tahiti, *Geophys. Res. Lett.*, *31*, L19103, doi:10.1029/2004GL020676.

Le Pichon, A., E. Blanc, D. Drob, S. Lambotte, J. X. Dessa, M. Lardy, P. Bani, and S. Vergniolle (2005), Infrasound monitoring of volcanoes to probe high-altitude winds, *J. Geophys. Res.*, *110*, D13106, doi:10.1029/2004JD005587.

Le Pichon, A., J. Vergoz, P. Herry, and L. Ceranna (2008), Analyzing the detection capability of infrasound arrays in Central Europe, *J. Geophys. Res.*, *113*, D12115, doi:10.1029/2007JD009509.

Le Pichon, A., J. Vergoz, E. Blanc, J. Guilbert, L. Ceranna, L. Evers, and N. Brachet (2009), Assessing the performance of the International Monitoring System's infrasound network: Geographical coverage and temporal variabilities, *J. Geophys. Res.*, *114*, D08112, doi:10.1029/2008JD010907.

Le Pichon, A., R. Matoza, N. Brachet, and Y. Cansi (2010), Recent enhancements of the PMCC infrasound signal detector, *Inframatics*, September 2010 issue, *26*, 5–8.

Matoza, R. S., A. Le Pichon, J. Vergoz, P. Herry, J. M. Lalande, H. Lee, I. Che, and A. Rybin (2011), Infrasonic observations of the June 2009 Sarychev Peak eruption, Kuril Islands: Implications for infrasonic monitoring of remote explosive volcanism, *J. Volcanol. Geotherm. Res.*, *200*, 35–48, doi:10.1016/j.jvolgeores.2010.11.022.

Walker, K. T., and M. A. H. Hedlin (2010), A review of wind-noise reduction methodologies, in *Infrasound Monitoring for Atmospheric Studies*, edited by A. L. Pichon, E. Blanc, and A. Hauchecorne, chap. 5, pp. 141–182, Springer, Netherlands.

Waxler, R., and K. E. Gilbert (2006), The radiation of atmospheric microbaroms by ocean waves, *J. Acoust. Soc. Am.*, *119*(5), 2651–2664, doi:10.1121/1.2191607.

Wilson, C. R., C. A. L. Szuberla, and J. V. Olson (2010), High-latitude observations of infrasound from Alaska and Antarctica: Mountain associated waves and geomagnetic/auroral infrasonic signals, in *Infrasound Monitoring for Atmospheric Studies*, edited by A. L. Pichon, E. Blanc, and A. Hauchecorne, chap. 13, pp. 415–454, Springer, Netherlands.